

# Evading Detector Backaction on a Quantum Cyclotron

X. Fan<sup>1, 2, \*</sup> and G. Gabrielse<sup>2, †</sup>

<sup>1</sup>*Department of Physics, Harvard University, Cambridge, Massachusetts 02138, USA*

<sup>2</sup>*Center for Fundamental Physics, Northwestern University, Evanston, Illinois 60208, USA*

(Dated: July 26, 2022)

The state of a one-particle quantum cyclotron can be detected by coupling it to a simple harmonic oscillator. The resulting quantum nondemolition (QND) detection comes at the price of a detector backaction that broadens the resonance lineshapes. The first quantum calculation of the coupled system shows that detection backaction can be evaded by resolving the quantum state of the detection oscillator.

The electron magnetic moment in Bohr magnetons, determined to 3 parts in  $10^{13}$ , is the most precisely determined property of an elementary particle [1, 2]. A better measurement is currently of great interest because of an intriguing, 2.4 standard deviation discrepancy [3] with the most precise prediction [4] of the Standard Model of particle physics (SM). Tests of the prediction are critical because these would check important elements of the SM – Dirac theory [5], quantum electrodynamics through the tenth order [4, 6, 7], hadronic contributions [8–10] and possible weak interaction contributions [10–14]. The SM prediction requires a measured fine structure constant,  $\alpha$ , as an input. This constant is determined from the measured Rydberg constant [15–17], atomic mass ratios [18–20], and atom recoil masses [21, 22]. The intriguing discrepancy has stimulated new theoretical investigations into possible physics beyond the SM [23–27].

A quantum cyclotron [28] is a single trapped electron that occupies only the ground and first excited states of its cyclotron motion. Quantum non-demolition (QND) detection of the state of this quantum cyclotron made past measurements possible. However, a detector backaction produced a broad cyclotron lineshape that limited the accuracy with which the cyclotron oscillation frequency could be determined. In this Letter, we present the possibility of evading the detector backaction to produce extremely narrow lineshapes for better measurements. A steady-state solution to a master equation provides the first quantum treatment of a quantum cyclotron coupled to a detection oscillator with a QND coupling. For promising quantum measurement conditions becoming available, the predicted lineshape differs dramatically from a previous prediction that assumed a classical detection oscillator [29, 30]. Calculation details, comparisons to Brownian motion lineshapes, and applications to other elements of electron and positron magnetic moment measurements are in a longer report [31].

The Hamiltonian for the quantum cyclotron [32, 33] with angular cyclotron frequency,  $\omega_c$ ,

$$H_c = \hbar\omega_c (a_c^\dagger a_c + \frac{1}{2}), \quad (1)$$

\* xingfan@g.harvard.edu

† gerald.gabrielse@northwestern.edu

has the form of a simple harmonic oscillator. The energy eigenvalues are a ladder of equally spaced Landau levels [32],  $\hbar\omega_c(n_c + 1/2)$  with  $n_c = 0, 1, 2, \dots$ . The raising and lowering operators,  $a_c^\dagger$  and  $a_c$ , in terms of position and momentum operators differs from that for a simple harmonic oscillator, of course, because circular rather than linear motion is described. For the same reason, the position representation of energy eigenstates  $|n_c\rangle$  are associated Laguerre polynomials rather than the Hermite polynomials for a simple harmonic oscillator.

QND detection of the quantum cyclotron state is possible if it is appropriately coupled to a harmonic oscillator that has a Hamiltonian,

$$H_z = \hbar\omega_z (a_z^\dagger a_z + \frac{1}{2}), \quad (2)$$

energy eigenstates  $|n_z\rangle$ , and eigenvalues  $\hbar\omega_z(n_z + 1/2)$ , with  $n_z = 0, 1, \dots$ . For an electron in the electrostatic quadrupole potential of a Penning trap, this detection motion is the axial oscillation of the electron along the magnetic field direction. The raising and lowering operators,  $a_z^\dagger$  and  $a_z$ , in terms of position and momentum operators are in every quantum mechanics textbook, as are the energy eigenstates in the position representation. The uncoupled cyclotron-plus-axial Hamiltonian

$$H_0 = H_c + H_z, \quad (3)$$

has  $|n_c, n_z\rangle = |n_c\rangle |n_z\rangle$  as energy eigenstates, and

$$E(n_c, n_z) = \hbar\omega_c(n_c + \frac{1}{2}) + \hbar\omega_z(n_z + \frac{1}{2}) \quad (4)$$

as energy eigenvalues. The representation in Fig. 1 is not to scale since  $\omega_c$  is typically 1000 times larger than  $\omega_z$ .

A QND coupling [34–36] of the two oscillators,

$$V = \hbar\delta_c (a_c^\dagger a_c + \frac{1}{2}) (a_z^\dagger a_z + \frac{1}{2}), \quad (5)$$

commutes with  $H_0$  and does not change the system state. In a Penning trap with uniform field  $B\hat{z}$ , the shift

$$\delta_c = \hbar e B_2 / (m^2 \omega_z), \quad (6)$$

comes from adding a magnetic bottle gradient [37]

$$\Delta B = B_2 (z^2 - \frac{1}{2}(x^2 + y^2)). \quad (7)$$

The Eq. (5) coupling pertains when two rapidly oscillating terms average to zero.

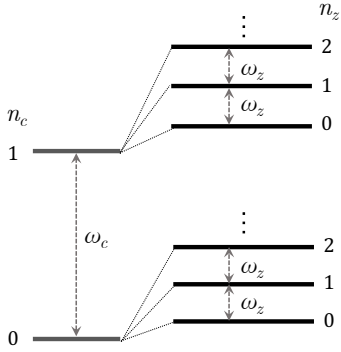


FIG. 1. Lowest energy levels for the combined quantum cyclotron and axial detection oscillator (not to scale).

The uncoupled states  $|n_c, n_z\rangle$  are also the eigenstates of the coupled Hamiltonian,

$$H = H_c + H_z + V. \quad (8)$$

Because of the coupling, the energy eigenvalues

$$E(n_c, n_z) = \hbar\omega_c(n_c + \frac{1}{2}) + \hbar\omega_z(n_z + \frac{1}{2}) + \hbar\delta_c(n_c + \frac{1}{2})(n_z + \frac{1}{2}), \quad (9)$$

acquire a small term that depends upon both  $n_c$  and  $n_z$ .

That this coupling provides the desired QND detection can be seen by writing the energy eigenvalues as

$$E(n_c, n_z) = \hbar(n_c + \frac{1}{2}) + \hbar\tilde{\omega}_z(n_z + \frac{1}{2}). \quad (10)$$

Measuring the effective axial frequency

$$\tilde{\omega}_z = \omega_z + \delta_c(n_c + \frac{1}{2}), \quad (11)$$

determines  $n_c$  without changing the cyclotron state. Quantum jump spectroscopy [28] can then determine the cyclotron frequency that is needed (along with another frequency) to determine the magnetic moment.

The undesirable and unavoidable detector backaction can be seen by writing the energy eigenvalues as

$$E(n_c, n_z) = \hbar\tilde{\omega}_c(n_c + \frac{1}{2}) + \hbar\omega_z(n_z + \frac{1}{2}). \quad (12)$$

This formulation emphasizes that the cyclotron frequency shifts from  $\omega_c$  to

$$\tilde{\omega}_c = \omega_c + \delta_c(n_z + \frac{1}{2}). \quad (13)$$

The backaction shifts the cyclotron frequency in proportion to the axial energy and quantum number. Any distribution of axial states is thereby turned into an undesirable distribution of effective cyclotron frequencies.

A distribution of axial states arises because the axial oscillator is weakly coupled to its environment, with a coupling constant,  $\gamma_z$ . For times larger than  $1/\gamma_z$ , this leads to a thermal Boltzmann distribution of axial states. For  $T = 0.1$  K and  $\omega_z/(2\pi) = 200$  MHz, the lowest ambient temperature and typical frequency used for

measurements[1, 2], the average axial quantum number is

$$\bar{n}_z = \left[ \exp\left(\frac{\hbar\omega_z}{k_B T}\right) - 1 \right]^{-1} \approx \frac{k_B T}{\hbar\omega_z} \approx 10. \quad (14)$$

For past measurements, the effective axial temperature was actually at least 3 to 5 times higher due to the elevated temperature of the electronics used to detect the axial oscillation and its frequency[2]. The broad cyclotron linewidth that resulted because of the detection backaction limited the accuracy of the measurements.

The cyclotron motion also weakly couples to the thermal reservoir, with a coupling  $\gamma_c$ . A state  $|n_c\rangle$  radiates synchrotron radiation at a rate  $n_c\gamma_c$ . In principle, cyclotron states can also absorb blackbody radiation, but at 0.1 K and  $\omega_c/(2\pi) = 150$  GHz[1], the number of available blackbody photons is negligible. The average quantum number for a Boltzmann distribution of states is

$$\bar{n}_c = \left[ \exp\left(\frac{\hbar\omega_c}{k_B T}\right) - 1 \right]^{-1} = 1.2 \times 10^{-32} \approx 0. \quad (15)$$

The cyclotron motion thus remains in its  $n_c = 0$  ground state [28] unless a cyclotron driving force is applied.

A cyclotron drive adds the Hamiltonian term

$$V_c(t) = \frac{1}{2}\hbar\Omega_c \left[ a_c^\dagger e^{-i(\omega_c + \epsilon_c)t} + a_c e^{i(\omega_c + \epsilon_c)t} \right]. \quad (16)$$

The drive strength is given by the angular Rabi frequency,  $\Omega_c$ , and the drive is detuned from resonance at  $\omega_c$  by a detuning  $\epsilon_c$ . For measurements, the driving force provided by 150 GHz microwaves injected into a trap cavity excites the  $|0, n_z\rangle$  states to  $|1, n_z\rangle$ . Higher cyclotron states can be neglected because it is less probable to excite from small population in an excited state, but also because a relativistic shift keeps the cyclotron transitions between excited states off resonance from the drive [38].

A density operator is required for a system that decays and is coupled to a thermal bath. The initial state at time  $t = 0$  is the cyclotron ground state and a thermal superposition of axial states,

$$\rho(0) = \sum_{n_z=0}^{\infty} p_{n_z}(T) |0, n_z\rangle \langle 0, n_z|. \quad (17)$$

The Boltzmann weighting factors are

$$p_n(T) = \left[ 1 - \exp\left(-\frac{\hbar\omega_z}{k_B T}\right) \right] \exp\left(-\frac{n\hbar\omega_z}{k_B T}\right). \quad (18)$$

Explicit calculations show that 150 axial states suffice for axial states in thermal equilibrium at 0.1 K.

The time evolution of the density operator is described by a Lindblad equation [39, 40],

$$\begin{aligned} \frac{d\rho}{dt} = & -\frac{i}{\hbar} [H_0 + V + V_c, \rho] \\ & - \frac{\gamma_c}{2} (a_c^\dagger a_c \rho - 2a_c \rho a_c^\dagger + \rho a_c^\dagger a_c) \\ & - \frac{\gamma_z}{2} \bar{n}_z (a_z a_z^\dagger \rho - 2a_z^\dagger \rho a_z + \rho a_z a_z^\dagger) \\ & - \frac{\gamma_z}{2} (\bar{n}_z + 1) (a_z^\dagger a_z \rho - 2a_z \rho a_z^\dagger + \rho a_z^\dagger a_z). \end{aligned} \quad (19)$$

The first line describes the driven motion. The second describes the incoherent cyclotron decay. The third and fourth lines describe the incoherent deexcitation and excitation of the axial motion by the thermal bath.

To efficiently solve the master equation, several transformations are made. All terms in Eq. (19) are transformed to an interaction picture. For example,

$$\tilde{\rho} = e^{iH_0 t/\hbar} \rho e^{-iH_0 t/\hbar}. \quad (20)$$

Since the coupled system starts and remains axially diagonal, only the probabilities  $\tilde{\rho}_{jk;n_z} = \langle j, n_z | \tilde{\rho} | k, n_z \rangle$  are needed. The indices  $j$  and  $k$  are 0 or 1, and  $n_z$  takes positive values as large as needed to describe the thermal distribution – up to about 150 for  $\bar{n}_z = 10$ , as mentioned.

A second transformation,

$$p_{jk;n_z} \equiv \rho_{jk;n_z} e^{i(j-k)\epsilon_c t} \quad (21)$$

produces a time-independent equation for the  $p_{jk;n_z}$ . The time-dependent probabilities we seek to calculate,

$$p_{jj;n_z} = \tilde{\rho}_{jj;n_z} = \langle j, n_z | \rho | j, n_z \rangle \quad (22)$$

are invariant under these transformations.

The master equation in terms of vectors  $\vec{p}_{jk}$ , with components  $p_{jk;n_z}$ , is

$$\begin{aligned} \frac{d}{dt} \vec{p}_{00}(t) &= \mathbf{R}(0, 0, 0) \vec{p}_{00}(t) - \Omega_c \text{Im} [\vec{p}_{01}(t)] \\ &\quad + \gamma_c \vec{p}_{11}(t) \end{aligned} \quad (23a)$$

$$\frac{d}{dt} \vec{p}_{01}(t) = \mathbf{R}(\epsilon_c, \delta_c, \gamma_c) \vec{p}_{01}(t) - i \frac{\Omega_c}{2} (\vec{p}_{11}(t) - \vec{p}_{00}(t)) \quad (23b)$$

$$\frac{d}{dt} \vec{p}_{11}(t) = \mathbf{R}(0, 0, 2\gamma_c) \vec{p}_{11}(t) + \Omega_c \text{Im} [\vec{p}_{01}(t)]. \quad (23c)$$

The nonzero components of the matrices are

$$\mathbf{R}(\epsilon, \delta, \gamma_c)_{n,n-1} = \gamma_z \bar{n}_z n \quad (24a)$$

$$\begin{aligned} \mathbf{R}(\epsilon, \delta, \gamma_c)_{n,n} &= i \left[ -\epsilon + (n + \frac{1}{2})\delta \right] - \frac{1}{2}\gamma_c \\ &\quad - \gamma_z (2\bar{n}_z + 1)n - \gamma_z \bar{n}_z \end{aligned} \quad (24b)$$

$$\mathbf{R}(\epsilon, \delta, \gamma_c)_{n,n+1} = \gamma_z (\bar{n}_z + 1)(n + 1). \quad (24c)$$

Beside the specified arguments and indices, these equations and matrices depend upon the bath temperature via  $\bar{n}_z$ , and the axial damping rate,  $\gamma_z$ .

This vector master equation must be solved for initial conditions (at  $t = 0$ ) that  $\vec{p}_{00}$  has components  $p_{n_z}(T)$  (from Eq. (17)) and  $\vec{p}_{01} = \vec{p}_{11} = 0$ . The desired resonance lineshape is the probability of a cyclotron excitation,

$$P = \sum_{n_z=0}^{\infty} p_{11;n_z}(t_d), \quad (25)$$

as a function of the drive detuning,  $\epsilon_c$ . This lineshape depends upon the drive strength,  $\Omega_c$  and the time that the drive is applied,  $t_d$ .

In general, the vector master equation must be integrated numerically from  $t = 0$  to  $t = t_d$  to determine the lineshape. However, for a weak drive with  $\Omega_c \ll \gamma_c$  (to avoid power broadening) and  $t_d \gg 1/\gamma_c$  (to let transients damp out), there is a steady state for which the driven cyclotron excitation balances the emission of synchrotron radiation. This steady-state solution suffices to demonstrate the possibility of detector backaction evasion.

To obtain the steady-state solution, the derivatives in Eq. (23) are set to zero. The three equations are summed over all axial states and simplified using

$$\sum_{n_z=0}^{\infty} p_{00;n_z}(t) \approx \sum_{n_z=0}^{\infty} p_{n_z}(T) = 1 \quad (26)$$

$$\sum_{n_z=0}^{\infty} p_{11;n_z}(t) \ll 1 \quad (27)$$

$$\sum_{n_z=0}^{\infty} (\mathbf{R}(0, 0, 2\gamma_c) \vec{p}_{11})_{n_z} = -\gamma_c \sum_{n_z=0}^{\infty} p_{11;n_z}, \quad (28)$$

The first two simplifications pertain for a weak drive and make terms involving  $\vec{p}_{11}$  negligible compared to those involving  $\vec{p}_{00}$ . The third pertains because  $\mathbf{R}(0, 0, 2\gamma_c)$  has a simple structure and axial damping does not change the total population in states  $|1, n_z\rangle$ . The result is the steady-state probability for cyclotron excitation by a weak drive,

$$P = -\frac{\Omega_c^2}{2\gamma_c} \text{Im} \left[ \sum_{n_z=0}^{\infty} (i\mathbf{R}(\epsilon_c, \delta_c, \gamma_c)^{-1} \vec{p}(T))_{n_z} \right]. \quad (29)$$

The vector  $\vec{p}(T)$  has the Boltzmann factors  $p_{n_z}(T)$  as its components.

For the limit  $T = 0$ , the steady-state lineshape for a weak drive becomes a Lorentzian,

$$P_0 = \left( \frac{\Omega_c}{\gamma_c} \right)^2 \frac{\left( \frac{1}{2}\gamma_c \right)^2}{\left( \epsilon_c - \frac{1}{2}\delta_c \right)^2 + \left( \frac{1}{2}\gamma_c \right)^2}. \quad (30)$$

Its full width at half maximum is  $\gamma_c$  and its maximum is shifted to  $\epsilon_c = \delta_c/2$  because of the axial zero point energy. The resonant probability is a very small fraction,  $(\Omega_c/\gamma_c)^2$ , given that the drive is weak. The Lorentzian comes about because only the lowest axial state is populated,  $\bar{n}_z = 0$ ,  $\vec{p}(T)$  collapses to a single element  $p_0(T) = 1$ , and only the reciprocal of  $\mathbf{R}_{00} = -i\epsilon_c + i\delta_c/2 - \frac{1}{2}\gamma_c$  contributes to Eq. (29).

Direct numerical integrations of the master equation (Eq. (23)) and the steady-state solution in Eq. (29) provide the first fully quantum treatment of the coupled cyclotron and axial system. (More details, including comparisons of direct integrations and steady-state solutions of the master equation, are in a longer work that deals with measuring magnetic moments more generally [31].) The lineshape calculation [29, 30] previously available (and used to predict and analyze all experiments to date) assumed a classical axial oscillation undergoing Brownian motion – producing a very different lineshape.

We now investigate detector backaction and its evasion, with estimates first, and then with quantum line-shape calculations. The result of a thermal distribution of axial states is that a cyclotron drive will make cyclotron transitions over a range of cyclotron drive frequencies,  $\Delta\epsilon_c > \bar{n}_z\delta_c$ . For the best measurement, the bath temperature was 0.3 K and above, which corresponds to a spread  $\Delta\omega/\omega_c > 800$  ppt (A part per trillion, ppt, is 1 part in  $10^{12}$ ). Line splitting made it possible to obtain a 300 ppt uncertainty. Even at 0.1 K temperature, the backaction linewidth will still spread the cyclotron excitation over a broad width. Reducing the coupling strength ( $\delta_c$  in Eq. (5)) would reduce the backaction. However, this is not an option because this simultaneously reduces the sensitivity needed to detect the individual states of the quantum cyclotron.

The new possibility proposed here is evading backaction by resolving the cyclotron excitations that an electron makes while it is in its axial ground state, distinguishing these from the broad range of excitations taking place while the system is in other axial states (estimated above). Resolving  $\delta_c$ , the cyclotron frequency shift for axial states with  $n_z = 0$  and  $n_z = 1$ , requires two conditions,

$$\delta_c \gg \gamma_c + 2\bar{n}_z\gamma_z \quad (31)$$

$$\delta_c \gg 1/t_d. \quad (32)$$

The first (from the diagonal damping term in Eq. (24b)) requires that the shift be larger than both the cyclotron damping width,  $\gamma_c$ , and the axial width contribution,  $2\bar{n}_z\gamma_z$ . The latter arises because the underlying physics of the master equation is that probability transfers between the axial oscillation and the thermal reservoir at an average rate going as  $\bar{n}_z\gamma_z$ . The second requirement is a drive applied long enough that the frequency-time uncertainty principle does not broaden the lineshape.

The shift  $\delta_c/(2\pi) = 4$  Hz used for measurements is much smaller than the extremely small cyclotron damping width,  $\gamma_c/(2\pi) = 0.03$  Hz, realized using a microwave cavity to inhibit spontaneous emission [41]. At the ambient temperature of experiments,  $T = 0.1$  K, this leaves means that  $\gamma_z/(2\pi) \ll 0.2$  Hz is needed. This requirement was not met by the  $\gamma_z/(2\pi) = 1$  Hz of the best measurement. Resolving axial quantum structure thus requires reducing  $\gamma_z$  by about two orders magnitude. The second condition (Eq. (32)) is met by simply applying the cyclotron drive for much longer than 40 ms.

The axial damping rate cannot be reduced by this large factor during the time that the frequency of the axial frequency is measured to determine the quantum state of the cyclotron motion (Eq. (11)). The detected signal is proportional to this damping rate, and a large value is required to detect the signal from a single particle. However, it seems possible to electronically switch the axial damping rate between a small value during the time that excitations are driven, and a large value for subsequent detection of the axial frequency [31].

Quantum calculations of the cyclotron lineshape

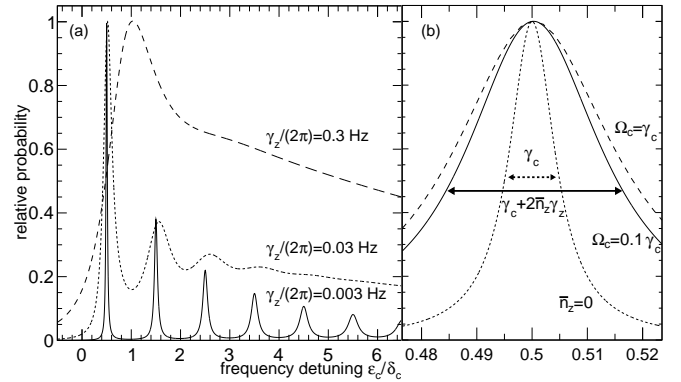


FIG. 2. (a) Quantum cyclotron lineshape for a weak drive ( $\Omega_c = 0.1\gamma_c$ ) resolves the axial states as the axial damping rates  $\gamma_z$  is reduced. (b) The  $n_z = 0$  peak for  $\gamma_z = 0.003$  Hz for a weak (solid curve) and strong drive (dashed), and a  $T = 0$  K Lorentzian lineshape (dotted).

demonstrate the backaction evasion. Figure 2(a) shows steady-state lineshapes (Eq. (29)) for three values of the axial damping rate,  $\gamma_z$ , at a temperature  $T = 0.1$  K and a coupling  $\delta_c/(2\pi) = 4$  Hz. For the dashed lineshape,  $2\bar{n}_z\gamma_z/(2\pi) = 6$  Hz does not satisfy Eq. (31) and the axial quantum states is not resolved. For a ten times lower  $\gamma_z/(2\pi) = 0.03$  Hz, the quantum structure of the axial motion manifests itself in the dotted lineshape. For another 10-fold reduction in  $\gamma_z$ , the solid lineshape shows completely resolved peaks.

The extremely narrow left peak for  $n_z = 0$  is good news for measurement. Its width,  $\gamma_c + 2\bar{n}_z\gamma_z$ , is only about 3 times the cyclotron decay width  $\gamma_c$ , and much smaller than the total cyclotron linewidth (Fig. 2(b)). More good news is that this  $n_z = 0$  peak is very symmetric about its center frequency – a big help in precisely identifying the center frequency of the resonance. The next peak to the right is for  $n_z = 1$ , and so on. There are many peaks because  $\bar{n}_z = 10$  for  $T = 0.1$  K.

The peak probability for a resonant weak drive,  $\Omega_c = 0.1\gamma_c$ , is only  $3.1 \times 10^{-4}$ . However, increasing the cyclotron drive strength to  $\Omega_c = \gamma_c$  (dashed curve in Fig. 2(b)) increases the excitation probability to  $2.2 \times 10^{-2}$  while power broadening the full linewidth from 3 to only 3.6 cyclotron decay widths. (The 300 differential equations for the vector master equation were integrated directly to time  $10/\gamma_c$  for  $\Omega_c = \gamma_c$  because the steady state solution applies only for  $\Omega_c \ll \gamma_c$ .) Stronger drives may be useful for tracking slow magnetic field drifts [2].

The offset of the  $n_z = 0$  resonance from  $\epsilon_c = 0$  to  $\epsilon_c = \delta_c/2$  is due to the zero point motion of the quantum axial oscillator. This could be measured in two ways. First, measuring this peak and its neighbor determines this offset, since these two peaks are spaced by twice the offset. Second, the shift of axial frequency  $\omega_z$  to  $\omega_z + \delta_c$  can be measured.

In summary, detector backaction that was thought to

limit the accuracy of electron magnetic moment measurements can be evaded. This is demonstrated using the first quantum mechanical treatment of a quantum cyclotron that has a QND coupling to a harmonic detection oscillation. The cyclotron resonance lineshapes that are predicted contain extremely narrow peaks that correspond

to resolved quantum states of the detection oscillation.

This work was supported by the NSF, with partial support of X. Fan from the Masason Foundation. B. D'Urso made early contributions. B. D'Urso, S. E. Fayer, T. G. Myers, B. A. D. Sukra and G. Nahal provided useful comments.

---

[1] D. Hanneke, S. Fogwell, and G. Gabrielse, *Phys. Rev. Lett.* **100**, 120801 (2008).

[2] D. Hanneke, S. Fogwell Hoogerheide, and G. Gabrielse, *Phys. Rev. A* **83**, 073002 (2011).

[3] G. Gabrielse, S. Fayer, T. Myers, and X. Fan, *Atoms* **7**, 45 (2019).

[4] T. Aoyama, T. Kinoshita, and M. Nio, *Atoms* **7**, (2019).

[5] P. A. M. Dirac and R. H. Fowler, *Proceedings of the Royal Society of London. Series A, Containing Papers of a Mathematical and Physical Character* **117**, 610 (1928).

[6] S. Laporta, *Physics Letters B* **772**, 232 (2017).

[7] T. Aoyama, T. Kinoshita, and M. Nio, *Phys. Rev. D* **97**, 036001 (2018).

[8] D. Nomura and T. Teubner, *Nucl. Phys. B* **867**, 236 (2013).

[9] A. Kurz, T. Liu, P. Marquard, and M. Steinhauser, *Physics Letters B* **734**, 144 (2014).

[10] Jegerlehner, Fred, *EPJ Web Conf.* **218**, 01003 (2019).

[11] K. Fujikawa, B. W. Lee, and A. I. Sanda, *Phys. Rev. D* **6**, 2923 (1972).

[12] A. Czarnecki, B. Krause, and W. J. Marciano, *Phys. Rev. Lett.* **76**, 3267 (1996).

[13] M. Knecht, M. Perrottet, E. de Rafael, and S. Peris, *Journal of High Energy Physics* **2002**, 003 (2002).

[14] A. Czarnecki, W. J. Marciano, and A. Vainshtein, *Phys. Rev. D* **67**, 073006 (2003).

[15] C. G. Parthey, A. Matveev, J. Alnis, B. Bernhardt, A. Beyer, R. Holzwarth, A. Maistrou, R. Pohl, K. Predehl, T. Udem, T. Wilken, N. Kolachevsky, M. Abgrall, D. Rovera, C. Salomon, P. Laurent, and T. W. Hänsch, *Phys. Rev. Lett.* **107**, 203001 (2011).

[16] H. Fleurbaey, S. Galtier, S. Thomas, M. Bonnaud, L. Julien, F. m. c. Biraben, F. m. c. Nez, M. Abgrall, and J. Guéna, *Phys. Rev. Lett.* **120**, 183001 (2018).

[17] A. Beyer, L. Maisenbacher, A. Matveev, R. Pohl, K. Khabarova, A. Grinin, T. Lamour, D. C. Yost, T. W. Hänsch, N. Kolachevsky, and T. Udem, *Science* **358**, 79 (2017).

[18] M. P. Bradley, J. V. Porto, S. Rainville, J. K. Thompson, and D. E. Pritchard, *Phys. Rev. Lett.* **83**, 4510 (1999).

[19] S. Sturm, F. Köhler, J. Zatorski, A. Wagner, Z. Harman, G. Werth, W. Quint, C. H. Keitel, and K. Blaum, *Nature* **506**, 467 (2014).

[20] E. Myers, *Atoms* **7**, 37 (2019).

[21] R. H. Parker, C. Yu, W. Zhong, B. Estey, and H. Müller, *Science* **360**, 191 (2018).

[22] R. Bouchendira, P. Cladé, S. Guellati-Khélifa, F. m. c. Nez, and F. m. c. Biraben, *Phys. Rev. Lett.* **106**, 080801 (2011).

[23] S. Gardner and X. Yan, *Light scalars with lepton number to solve the  $(g-2)_e$  anomaly*, 2019.

[24] J. Liu, C. E. M. Wagner, and X.-P. Wang, *Journal of High Energy Physics* **2019**, 8 (2019).

[25] H. Davoudiasl and W. J. Marciano, *Phys. Rev. D* **98**, 075011 (2018).

[26] A. Crivellin, M. Hoferichter, and P. Schmidt-Wellenburg, *Phys. Rev. D* **98**, 113002 (2018).

[27] X.-F. Han, T. Li, L. Wang, and Y. Zhang, *Phys. Rev. D* **99**, 095034 (2019).

[28] S. Peil and G. Gabrielse, *Phys. Rev. Lett.* **83**, 1287 (1999).

[29] L. S. Brown, *Phys. Rev. Lett.* **52**, 2013 (1984).

[30] L. S. Brown, *Ann. Phys. (N.Y.)* **159**, 62 (1985).

[31] X. Fan and G. Gabrielse, *(Manuscript in preparation.)* (2020).

[32] L. Landau, *Zeitschrift für Physik* **64**, 629 (1930).

[33] L. S. Brown and G. Gabrielse, *Rev. Mod. Phys.* **58**, 233 (1986).

[34] V. B. Braginsky, Y. I. Vorontsov, and K. S. Thorne, *Science* **209**, 547 (1980).

[35] C. M. Caves, K. S. Thorne, R. W. P. Drever, V. D. Sandberg, and M. Zimmermann, *Rev. Mod. Phys.* **52**, 341 (1980).

[36] V. B. Braginsky and F. Y. Khalili, *Rev. Mod. Phys.* **68**, 1 (1996).

[37] R. Van Dyck, Jr., P. Ekstrom, and H. Dehmelt, *Nature* **262**, 776 (1976).

[38] G. Gabrielse, H. Dehmelt, and W. Kells, *Phys. Rev. Lett.* **54**, 537 (1985).

[39] G. Lindblad, *Comm. Math. Phys.* **48**, 119 (1976).

[40] V. Gorini, A. Kossakowski, and E. C. G. Sudarshan, *Journal of Mathematical Physics* **17**, 821 (1976).

[41] G. Gabrielse and H. Dehmelt, *Phys. Rev. Lett.* **55**, 67 (1985).